Strength, stiffness, and microstructure of Cu(In,Ga)Se2 thin films deposited via sputtering and co-evaporation

Shi Luo, Jiun-Haw Lee, Chee-Wee Liu, Jia-Min Shieh, Chang-Hong Shen, Tsung-Ta Wu, Dongchan Jang, and Julia R. Greer

Citation: Applied Physics Letters **105**, 011907 (2014); doi: 10.1063/1.4890086
View online: http://dx.doi.org/10.1063/1.4890086
View Table of Contents: http://scitation.aip.org/content/aip/journal/apl/105/1?ver=pdfcov
Published by the AIP Publishing

Strength, stiffness, and microstructure of Cu(In,Ga)Se2 thin films deposited via sputtering and co-evaporation

Shi Luo,[1] Jiun-Haw Lee,[2] Chee-Wee Liu,[3] Jia-Min Shieh,[4] Chang-Hong Shen,[4] Tsung-Ta Wu,[4] Dongchan Jang,[1] and Julia R. Greer[1,a)]
[1]*Division of Applied Science and Engineering, California Institute of Technology, 1200 E California Blvd., Pasadena, California 91125, USA*
[2]*Graduate Institute of Photonics and Optoelectronics and Department of Electrical Engineering, National Taiwan University, No. 1, Sec 4 Roosevelt, Taipei 10617, Taiwan*
[3]*Department of Electrical Engineering, National Taiwan University, No 1, Sec 4 Roosevelt, Taipei 10617, Taiwan*
[4]*National Nano Device Laboratories, Hsinchu Science Park, No. 26, Prosperity Road I, Hsinchu 30078, Taiwan*

(Received 9 May 2014; accepted 22 June 2014; published online 10 July 2014)

This work examines $Cu(In,Ga)Se_2$ thin films fabricated by (1) selenization of pre-sputtered Cu-In-Ga and (2) co-evaporation of each constituent. The efficiency disparity between films deposited via these two methods is linked to differences in morphology and microstructure. Atomic force microscopy and scanning electron microscopy show that selenized films have rougher surfaces and poor adhesion to molybdenum back contact. Transmission electron microscopy and electron energy loss spectroscopy revealed multiple voids near the Mo layer in selenized films and a depletion of Na and Se around the voids. Residual stresses in co-evaporated films were found to be ~1.23 GPa using wafer curvature measurements. Uniaxial compression experiments on 500 nm-diameter nanopillars carved out from co-evaporated films revealed the elastic modulus of 70.4 ± 6.5 GPa. Hertzian contact model applied to nanoindentation data on selenized films revealed the indentation modulus of 68.9 ± 12.4 GPa, which is in agreement with previous reports. This equivalence of the elastic moduli suggests that microstructural differences manifest themselves after the yield point. Typical plastic behavior with two distinct failure modes is observed in the extracted stress-strain results, with the yield strength of 640.9 ± 13.7 MPa for pillars that failed by shearing and 1100.8 ± 77.8 MPa for pillars that failed by shattering. © *2014 AIP Publishing LLC*. [http://dx.doi.org/10.1063/1.4890086]

$Cu(In,Ga)Se_2$ (CIGS) has become one of the most promising materials for thin film photovoltaics, with recent achievement in efficiency of over 20% on soda lime glass (SLG) substrates[1] compared with traditional polycrystalline silicon cells.[2] The thin film nature of CIGS makes it suitable for depositing onto lightweight flexible substrates like polyimide films and metal foils, and amenable to roll-to-roll processing, with efficiencies of 18.7% reported for CIGS on Polyimide (PI) films[3] and of 17.9% on titanium foils.[4] Current studies of CIGS solar cells have been focused on improving the fabrication process and on fine-tuning cell parameters to achieve better device performance.[5] A scarcity of literature dedicated to the microstructure-properties connection for CIGS highlights the necessity to develop a fundamental understanding of this relationship to optimize device performance. Such analysis is particularly needed to understand the apparent disparity in performance between Cu-In-Ga-Se devices fabricated by two different processes: (1) co-evaporation of each individual constituent and (2) selenization of pre-sputtered Cu-In-Ga mixture. The latter has superior economic potential but its performance has been measured to be ~3/4 of that for the co-evaporated cells.[6]

This work presents microstructural and mechanical characterization of 1.5 μm-thick CIGS films deposited by co-evaporation and selenization with the goal of developing a better fundamental understanding of the CIGS material and of the effects of material processing on device performance.

Two separate batches of multilayered thin films were created using these processes. The absorber layer was deposited on a 700 nm-thick molybdenum back contact layer sputtered on SLG substrate in a two-steps process. Selenized films did not contain Ga; it is reasonable to assume that the mechanical and structural properties of $CuInSe_2$ (CIS) are similar to those of CIGS because their lattice structures are virtually equivalent.[7] Film thicknesses were measured using Scanning Electron Microscopy (SEM) to be 1.6 ± 0.2 μm for selenized films and 1.7 ± 0.1 μm for co-evaporated ones. Fabrication details and Electron Dispersive Spectroscopy (EDS) measurements can be found in Supplemental Material (SM) (or SI?).[6]

Fig. 1 shows SEM images of the selenized film (Figs. 1(a), 1(c), and 1(e)) and AFM profiles of the co-evaporated film (Figs. 1(b), 1(d), and 1(f)). The former appears to have a faceted grain structure, which contributes to the surface roughness. Cross-sectional images (Figs. 1(c) and 1(d)) suggest that selenized films did not adhere well to the underlying Mo and contained multiple voids and buckle-like gaps between the film and the substrate. Figs. 1(e) and 1(f) show AFM images of both films' surfaces obtained using Hysitron TI-950 nanoindenter with a standard Berkovich tip. Average roughness was recorded at 173.5 ± 17.1 nm for the selenized film, almost an order of magnitude rougher than 33.5 ± 4.3 nm in the co-evaporated film. Grains in co-evaporated films appear

a)Author to whom correspondence should be addressed. Electronic mail: jrgreer@caltech.edu

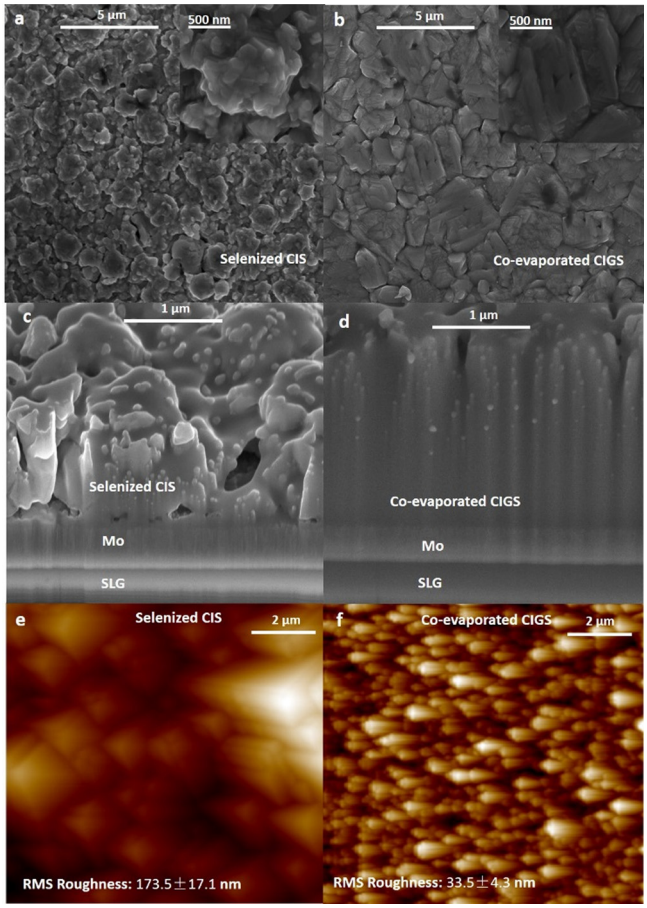

FIG. 1. Representative SEM images of (a) selenized CIS and (b) co-evaporated CIGS films taken top down with the zoomed-in view of the center location shown in the inset in the top right corner; and cross-section views of (c) selenized CIS and (d) co-evaporated CIGS films taken at 52°. AFM images in (e) and (f) correspond to the same films. For the RMS roughness values, measurements over 10 different regions on the same film were used for each type of films.

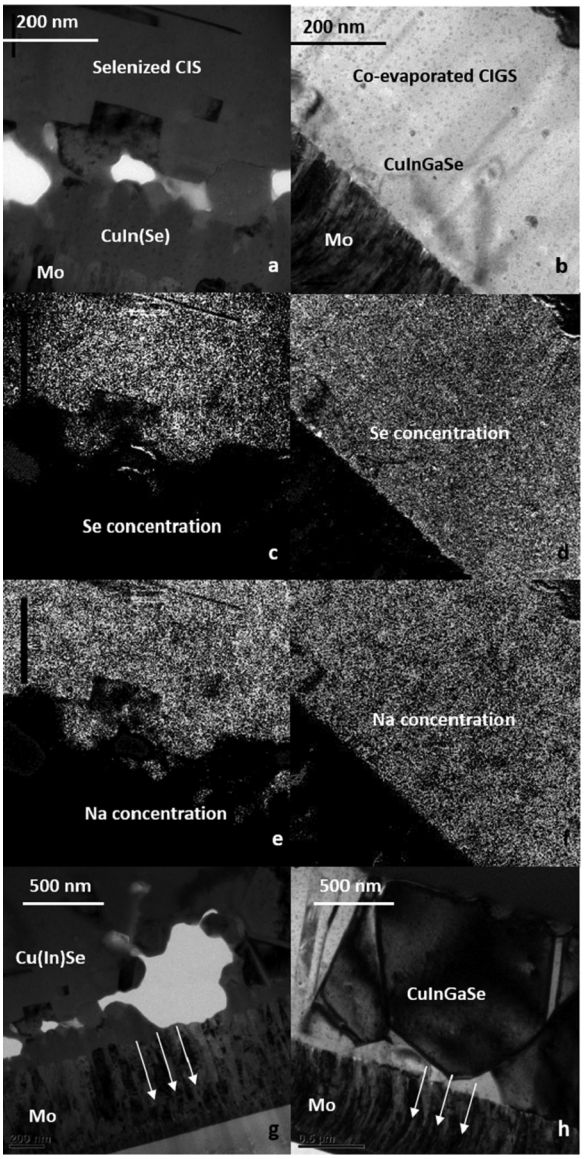

FIG. 2. Bright field TEM image of (a) and (g) selenized and (b) and (h) co-evaporated films; Se concentration of (c) selenized and (d) co-evaporated films; and Na concentration of (e) selenized and (f) co-evaporated films. Bending of columnar Mo grains can be observed in co-evaporated films but not in selenized ones, as shown by the arrows in (g) and (h). Note that in (a), the CuIn(Se) region does not contain Se, hence the different notation.

slender and anisotropic, while the selenized films appear faceted and isotropic with visibly larger variation in grain sizes (Fig. 1(a)).

Fig. 2 shows bright field TEM images of the cross-sections and EELS concentration maps for Se and Na for both films. TEM images reveal that grain sizes in the co-evaporated film were uniformly distributed around 1 μm, while distribution of grain sizes in the selenized film was broad, from 50 nm to 2 μm. Multiple ~200 nm-diameter voids were observed in the selenized film close to the interface with the Mo layer. Concentration profiles of Se and Na revealed a depletion region in the selenized film at ~100 nm above the interface, which coincides with the location of the voids. In the co-evaporated samples, Se and Na were homogeneously distributed throughout the thickness of the film. SEM and TEM images also revealed columnar grains in the Mo films, which were vertically bent in the co-evaporated films and not in the selenized ones.

Substrate curvature induced in the co-evaporated samples upon cooling to room temperature was measured by laser interferometry to estimate the residual stress in the film using Stoney's Formula (Eq. (1)),[8] using the assumption that stress state in the film is equibiaxial

$$\sigma_f = \left(\frac{E_s}{1-\nu_s}\right)\frac{t_s^2}{6t_f}K, \tag{1}$$

where σ_f is the stress after thin film deposition, E_s, ν_s and t_s are the Young's modulus, Poisson's ratio and thickness of the substrate, t_f is the thickness of the thin film, and K is the average of the measured radius of curvature of the sample in two orthogonal directions. Details on applying Stoney's Formula to multi-stack thin films can be found in supplementary material.[6] The average bending radii of the substrate were measured on 3 sets of samples: (1) as-fabricated SLG substrates which had dimensions of 2cm × 2cm × 2mm, (2) SLG substrates produced from the same batch as in (1) with 700 nm thick Mo films deposited via a two-step sputtering process, first at 150 °C, and second at 550 °C, and (3) same SLG substrates with 700 nm-thick Mo film and 1.5 μm-thick CIGS film evaporated on top of the stack at 550 °C. The

approximation of equibiaxial stress has been shown to be robust for many material systems in thin film on a rigid substrate form.[9] Since the actual stress in the film will likely be more complex, it underestimate the overall residual stress in the film because all out-of-plane and shear component of the stress vanish under the equibiaxial assumption. Calculated biaxial thin film stresses σ_f increased from 14.7 MPa (tensile) to −1.23 GPa (compressive) after co-evaporation. Substantial surface roughness in the selenized films prevented conducting similar curvature measurements.

Cylindrical nano-pillars were milled out from the co-evaporated films using Focused Ion Beam (FIB) and then compressed with a custom-fabricated 8 μm-diameter diamond flat punch in a nanoindenter. The pillar compression methodology and data analysis closely follow Greer[10] and Lee,[11] and relevant details can be found in supplementary material.[6] Stress-strain data with SEM images before and after deformation for a typical CIGS nano-pillar are shown in Fig. 3. Young's modulus was calculated to be 70.4 ± 6.5 GPa from the Continuous Stiffness Measurements (CSM) data once the contact has been firmly established,[6] which agrees with previously reported value of 73.4 GPa by Lin *et al.*[12] and the bulk modulus for single crystalline CIGS measured by X-ray Absorption Spectroscopy of 72 ± 2 GPa.[13] All pillars exhibited post-elastic flow, with the yield stresses ranging from 631.2 to 1151.5 MPa.

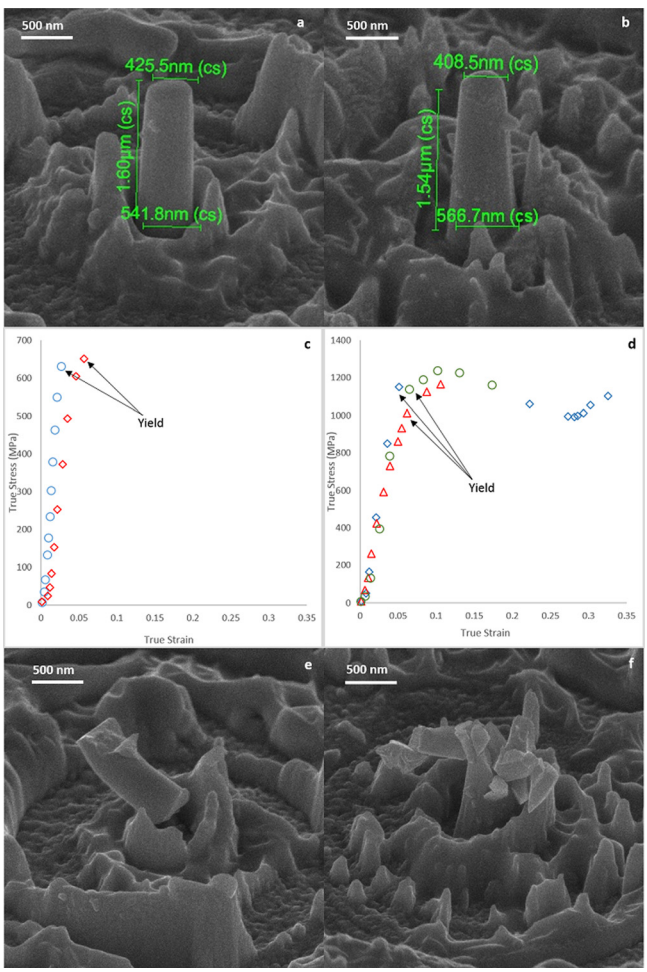

FIG. 3. SEM images of 500 nm diameter nanopillars before (a) and (b) and after (e) and (f) compression. (c) and (d) show the two representative types of stress strain behavior in terms of loading portions of true stress-strain curves, where, in (c), the pillars failed plastically near the bottom and, in (d), they shattered during compression. The identified yield points are shown on individual curves.

The substantial roughness and porosity in selenized CIGS prevented fabrication of nanopillars from these films. We used nanoindentation to determine the reduced modulus and stiffness of the selenized films and analyzed the elastic loading data via Hertzian contact model,[14] with the deforming grain and the tip of the indenter approximated as elastically contacting spheres. Indentation was conducted using a Berkovich tip with an effective radius of curvature R_1 of 150 nm;[15] the radius of the contacting grains R_2 was estimated from SEM images to be 500 ± 42 nm. Grains that are significantly larger than the average grain size in the film were intentionally selected under the optical microscope prior to indentation to better approximate spherical contact. An effective radius R was calculated as $\frac{1}{R} = \frac{1}{R_1} + \frac{1}{R_2}$ and inserted into the Hertzian contact model (Eq. (2)) along with the measured load-displacement data, F and d, to calculate the isotropic reduced modulus of the film, E_r

$$\mathrm{d} = \left(\frac{9F^2}{16RE_r^2}\right)^{\frac{1}{3}}. \tag{2}$$

A reduced modulus of 68.9 ± 12.4 GPa was obtained from 9 data sets. Caution should be taken when interpreting the Hertzian treatment because it assumes isotropic elasticity, whereas the CIGS film is polycrystalline and anisotropic, and because it approximates the grains to be perfect spheres. Depending on the actual contact geometry and orientation of the sample surface such approximation would potentially result in both over- and under-estimation of the reduced modulus.

Several morphological and micro-structural factors might contribute to the disparity in electrical performance between devices made with selenized and co-evaporated films. SEM and AFM surface profiles shown in Fig. 1 convey that the surface roughness in selenized films is an order of magnitude higher than that in the co-evaporated ones. This would affect the deposition of the CdS buffer layer and cause a poor contact at the CIGS/CdS interface.[16] The region near the interface with Mo shows partial delamination and voids within the CIGS film. Similar voids have been observed and were associated with the low Se flow rate during selenization process.[16] Our analysis for residual stress suggests they could also be mechanical in origin, as a result of buckling from high compressive stress in the CIGS film.[17] These voids and delamination would have an adverse effect on the mechanical integrity of the film and would eventually affect the device operational reliability.[18]

Fig. 2 shows an EELS compositional analysis within the cross-section of the sputtered CIGS film along its height. This image shows that the film is depleted in the Se and Na and consists entirely of Cu and In in the vicinity of the Mo layer and around the voids. In contrast, both Se and Na were homogeneously distributed in the co-evaporated film, with no observable depletion region.

The effect of the depletion region on device performance may be significant. While the Cu-In mixture without Se

will not be able to function properly, the lack of Se near the Mo layer also results in the absence of the $MoSe_2$ intermediate layer. The $MoSe_2$ usually located near the CIGS/Mo interface has been reported to be responsible for a significant efficiency increase by creating a quasi-ohmic contact between CIGS and Mo layer.[19] Na has long been identified as a critical constituent for the functionality and efficiency of CIGS operation and often associated with improved open circuit voltages and fill factors.[20] Na incorporation has also been reported to be crucial in governing absorber morphology and grain growth,[21] although a quantified optimal amount of Na has yet to be found, with contradictory observations reported.[22–24] It has been proposed that Na mainly exists in CIGS as substitutional point defect at Cu and In vacancy sites and alter the dopant concentration and bandgap by introducing acceptor-type defect complex such as Na_{In}.[25] Other reports show that Na has a strong preference for the charge-neutral Cu substitution and affects the electronic properties indirectly by means such as introducing new diffusion pathways.[26] Despite inconsistent reports, microstructural defects such as the observed Se/Na/$MoSe_2$ depletion region will likely affect the carrier transport near the Mo back contact in selenized CIGS films, and possibly contribute to the inferior performance observed in devices made with selenized cells.

Grain size has also been shown to affect device performance of CIGS, although no quantified correlation has been established because increasing[27] and decreasing[28] grain sizes within a certain range have both been reported to improve device performance. Nonetheless, it is generally agreed that larger grain sizes lead to greater carrier diffusion lengths and reduced recombination at grain boundaries.[29] TEM measured grain size in the co-evaporated films is considerably larger and more uniform than that for the selenized films, which could also be a factor in the device performance.

Residual stress analysis for the co-evaporated films reveals nearly 100-fold increase in compressive stress after the deposition of CIGS onto the Mo layer. Prior to depositing CIGS, the stress in Mo layer was tensile, at 14.7 MPa, on the same order as previously reported.[17] The stress increased by several orders of magnitude, to −1.23 GPa after the co-evaporation, with negative values indicating a compressive stress. Vertical bending of the columnar grains in the Mo layer is visible in the TEM images of the co-evaporated films and is consistent with the high residual stress in the film. Images of the as-deposited Mo layer without CIGS and Mo layer in the selenized films do not show significant grain bending, which suggests that the residual stress is likely a result of the difference between deposition conditions for selenized and co-evaporated films: Cu and In in the selenized films were sputtered onto the Mo layer at 150 °C, while for co-evaporated film, Cu-In-Ga-Se were deposited onto the film at a higher temperature of 550 °C, as detailed in supplementary material.[6] Mo layers in both samples were at room temperature after the previous deposition step. During the co-evaporation process Cu-In-Ga-Se mixture came in contact with the Mo layer at 550 °C, and subsequent cooling down to room temperature caused a significant thermal mismatch between the two films, which resulted in the development of misfit strains and greater residual stresses in the co-evaporated CIGS films. This is consistent with the observation of Mo thin film bending only in the co-evaporated films.

Excessive residual stress in the CIGS films will adversely affect the film micro-structure, as evidenced by the voids, delamination, and bending of Mo layer revealed by the SEM and TEM images. These would, in turn, impact the cell performance by affecting distribution of Se and Na across the film and would also lead to reliability concerns for commercial applications. Excessive residual stresses may also lead to premature mechanical failure in devices fabricated on thinner and flexible substrates such as foil/polymer. It has also been reported that high residual stresses in the Mo would change the orientation of selenized CIGS film deposited on top of it from the original preferred orientation (112) to (220)/(204) and, thus, change its crystallinity and affect device performance.[17] Decreasing the deposition temperature could potentially alleviate the high residual stress, but has been reported to have a concomitant adverse effect on grain growth and film quality.[16,30] As such, the residual stress appears to be a trade-off between better film quality and a more efficient production process. Further understanding on the origin of the stress is needed in order to develop effective means of reducing the stress level in the films.

Elastic properties are important in calculating the effects of temperature and pressure on the chalcopyrite family of semiconductors such as CIGS. Such calculations are of particular importance as CIGS has been shown to go through phase transformation to cubic under high temperature and working pressure.[13] Here, mechanical properties of CIGS were obtained from compression experiments on 500 nm-diameter nanopillars FIB-milled from co-evaporated films. The Young's modulus for co-evaporated films was calculated to be 70.4 ± 6.5 GPa, which is close to the reduced modulus value of 68.9 ± 12.4 GPa obtained for selenized films using Hertzian contact theory. Two distinct failure modes can be identified from SEM images of pillars before and after compression. Two out of five pillars failed by shearing near the bottom, while the other three shattered during compression. The stress strain curves are plotted according to these two categories and shown in Figs. 3(c) and 3(d). Only the loading part is shown as all pillars failed plastically, making it undesirable to try to extract information from the unloading part. All pillars show distinctive compression response for plastic materials such as large strain bursts. For pillars that failed near the bottom, the stress strain curve show typical brittle plastic failure, with a yield stress of 640.9 ± 13.7 MPa; for pillars that shattered, plastic deformation was observed after yielding happened at 1100.8 ± 77.8 MPa. The largest amount of plastic strain observed was 5%, and the corresponding yield stress is the highest of all pillars, reaching 1151.5 MPa. Non-perfect alignment between pillar and flat punch could result in the pillars shearing near the bottom, and also explain the lower yield stress observed. The significant plastic deformation and hardening and the resulting increase in yield stress observed in some of the tests also suggest that CIGS process some degree of ductility.

In summary, micro-structural and mechanical properties of Cu(In,Ga)Se2 thin films deposited on top of molybdenum back contact and soda lime glass substrate by two different techniques: selenization of Cu-In mixture, and co-evaporation,

were investigated. We found that selenized films have coarser and irregularly sized grains and suffer from voids and partial delamination from the Mo layer. Their surface roughness is also an order of magnitude higher compared to co-evaporated films. Multiple voids of diameter ~200 nm were observed near the Mo contact in selenized films. The region around these voids are depleted of Se and Na, and would lead to the disparity in device performance between selenized and co-evaporated films. High compressive stress was discovered in the co-evaporated films, which is in accordance with the bending of Mo layer observed in SEM and TEM images. A reduced modulus value of 68.9 ± 12.4 GPa was extracted using nanoindentation and Hertzian elastic contact model for selenized films. Compression of nanopillars 500 nm in diameter milled from co-evaporated films revealed an elastic modulus value of 70.4 ± 6.5 GPa and show good agreement with nanoindentation results for selenized films. All pillars show distinctive response of plastic material, and two failure modes (1) shearing near the bottom of the pillar and (2) shattering were observed. Yield stress for sheared pillars was measured as 640.9 ± 13.7 MPa, while plastic deformation and hardening was observed in shattered pillars, and a yield stress of 1100.8 ± 77.8 MPa was measured.

The authors gratefully acknowledge the financial support of the National Science Council of Taiwan through its Grant No. NSC 101-3113-P-008-001.

[1]P. Jackson, D. Hariskos, E. Lotter, S. Paetel, R. Wuerz, R. Menner, W. Wischmann, and M. Powalla, Prog. Photovoltaics Res. Appl. **19**, 894 (2011).
[2]M. Green and K. Emery, Prog. Photovoltaics Res. Appl. **20**(1), 12 (2012).
[3]A. Chirilă, S. Buecheler, F. Pianezzi, P. Bloesch, C. Gretener, A. R. Uhl, C. Fella, L. Kranz, J. Perrenoud, S. Seyrling, R. Verma, S. Nishiwaki, Y. E. Romanyuk, G. Bilger, and A. N. Tiwari, Nat. Mater. **10**, 857 (2011).
[4]T. Nakada, T. Yagioka, K. Horiguchi, T. Kuraishi, and T. Mise, in *Proceedings Of the 24th European Photovoltaics Solar Energy Conference* (IEEE, 2009), pp. 2425–2428.
[5]F. Kessler and D. Rudmann, Sol. Energy **77**, 685 (2004).
[6]See supplementary material at http://dx.doi.org/10.1063/1.4890086 for more information on experimental and fabrication details, for analysis of nanopillar compression, and for EDS and electrical measurements.
[7]A. S. Verma, S. Sharma, R. Bhandari, B. K. Sarkar, and V. K. Jindal, Mater. Chem. Phys. **132**, 416 (2012).
[8]G. G. Stoney, Proc. R. Soc. Lond. A **82**, 172 (1909).
[9]X. Feng, Y. Huang, and A. J. Rosakis, J. Appl. Mech. **74**, 1276 (2007).
[10]J. R. Greer, W. C. Oliver, and W. D. Nix, Acta Mater. **53**, 1821 (2005).
[11]S.-W. Lee, S. M. Han, and W. D. Nix, Acta Mater. **57**, 4404 (2009).
[12]Y.-C. Lin, X.-Y. Peng, L.-C. Wang, Y.-L. Lin, C.-H. Wu, and S.-C. Liang, J. Mater. Sci.: Mater. Electron. **25**(1), 461–465 (2013).
[13]C. Rincón, I. Villareal, and H. Galindo, J. Appl. Phys. **86**, 2355 (1999).
[14]H. Hertz, J. Die Reine Angew. Math. **92**, 156 (1881).
[15]Hysitron, *Hysitron TI 950 TriboIndenter User Manual* (2012).
[16]C.-H. Huang, Y. C. Shih, W.-J. Chuang, and C.-P. Lin, in *2010 10th IEEE International Conference on Solid-State Integrated Circuit Technology* (IEEE, 2010), pp. 2019–2021.
[17]T.-Y. Lin, C. Chen, and C.-H. Lai, in *2012 38th IEEE Photovoltaics Specialists Conference* (IEEE, 2012), pp. 001999–002002.
[18]D.-C. Perng, M.-C. Hung, and K.-Y. Wang, in *2012 38th IEEE Photovoltaics Specialists Conference* (IEEE, 2012), pp. 000891–000894.
[19]D. Abou-Ras, G. Kostorz, D. Bremaud, M. Kälin, F. V. Kurdesau, A. N. Tiwari, and M. Döbeli, Thin Solid Films **480–481**, 433 (2005).
[20]K. Granath, M. Bodegård, and L. Stolt, Sol. Energy Mater. Sol. Cells **60**, 279 (2000).
[21]D. Rudmann, A. F. da Cunha, M. Kaelin, F.-J. Haug, H. Zogg, and A. N. Tiwari, in *MRS Online Proceedings Library* (Cambridge Journals Online, 2003).
[22]M. A. Contreras, B. Egaas, P. Dippo, J. Webb, J. Granata, K. Ramanathan, S. Asher, A. Swartzlander, and R. Noufi, in *26th IEEE Photovoltaics Specialists Conference-1997* (IEEE, 1997), pp. 359–362.
[23]D. Rudmann, G. Bilger, M. Kaelin, F.-J. Haug, H. Zogg, and A. N. Tiwari, Thin Solid Films **431–432**, 37 (2003).
[24]T. Nakada, H. Ohbo, M. Fukuda, and A. Kunioka, Sol. Energy Mater. Sol. Cells **49**, 261 (1997).
[25]X. Sun, F. Jiang, and J. Feng, Comput. Mater. Sci. **47**, 31 (2009).
[26]L. E. Oikkonen, M. G. Ganchenkova, A. P. Seitsonen, and R. M. Nieminen, J. Appl. Phys. **114**, 083503 (2013).
[27]D. Rudmann, A. F. da Cunha, M. Kaelin, F. Kurdesau, H. Zogg, A. N. Tiwari, and G. Bilger, Appl. Phys. Lett. **84**, 1129 (2004).
[28]S. Ishizuka, A. Yamada, K. Matsubara, P. Fons, K. Sakurai, and S. Niki, Appl. Phys. Lett. **93**, 124105 (2008).
[29]W. Shafarman and J. Zhu, Thin Solid Films **362**, 473 (2000).
[30]S. Niki, M. Contreras, I. Repins, M. Powalla, K. Kushiya, S. Ishizuka, and K. Matsubara, Prog. Photovoltaics Res. Appl. **18**, 453 (2010).